JOURNAL OF SOLID STATE CHEMISTRY 118, 241–246 (1995)

Synthesis, Structure, and Magnetism of $BaVO(PO_4)(H_2PO_4) \cdot H_2O$, a New Layered Barium Vanadium(IV) Phosphate Hydrate

William T. A. Harrison,* Shiao C. Lim,* Laurie L. Dussack,* Allan J. Jacobson,* David P. Goshorn,† and Jack W. Johnson†

*Department of Chemistry, University of Houston, Houston, Texas 77204-5461; and †Corporate Research Laboratories, Exxon Research and Engineering Company, Annandale, New Jersey 08801

Received January 12, 1995; accepted March 14, 1995

The hydrothermal synthesis, X-ray single crystal structure, and some properties of $BaVO(PO_4)(H_2PO_4) \cdot H_2O$ are described. $BaVO(PO_4)(H_2PO_4) \cdot H_2O$ is built up from VO_6 and $(H_2)PO_4$ groups, linked via V–O–P bonds, into anionic $VO(PO_4)(H_2PO_4)$ layers. The 9-coordinate Ba^{2+} cations and water molecules provide the interlayer packing between the V/P/O/H sheets. Magnetic susceptibility measurements on $BaVO(PO_4)(H_2PO_4) \cdot H_2O$ show perfect Curie–Weiss paramagnetism down to 4 K. Powder X-ray, TGA, and IR data for $BaVO(PO_4)(H_2PO_4) \cdot H_2O$ are also presented. Crystal data: $BaVO(PO_4)(H_2PO_4) \cdot H_2O$, $M = 414.24$, monoclinic, space group $P2_1/n$ (No. 14), $a = 10.848$ (3) Å, $b = 6.408(3)$ Å, $c = 11.376(2)$ Å, $\beta = 102.32(2)°$, $V = 773(2)$ Å^3, $Z = 4$, $R(F) = 2.24\%$, $R_w(F) = 2.42\%$ [141 parameters; 2103 reflections with $I > 3\sigma(I)$].

INTRODUCTION

A number of phases in the barium/vanadium/phosphorus/oxygen (BaVPO) phase space have been previously characterized by single-crystal diffraction, including the layered vanadium(V)-containing $Ba(VO_2)PO_4$ (1), the channel-containing vanadium(IV) material $BaV_2P_2O_{10}$ (2), and the V(III)-containing phases $BaV_2P_4O_{14}$ (3), $Ba_2V_3H(PO_4)_2(P_2O_7)_2$, (4) and $BaV_2(HPO_4)_4 \cdot H_2O$ (5). These last three vanadium(III) materials all contain different, vertex-sharing, three-dimensional $VO_6/(H)PO_4$ frameworks.

We have reported new V(IV)-containing BaVPOs, including $Ba_8(VO)_6(HPO_4)_{11}(PO_4)_2 \cdot 3H_2O$ (6), which contains a complex arrangement of two different types of one-dimensional chains of vertex-sharing VO_6 and $(H)PO_4$ groups, separated by 10- and 13-coordinate barium cations, and $Ba_2VO(PO_4)_2 \cdot H_2O$ (7), which contains one-dimensional $VO(PO_4)_2 \cdot H_2O$ chains, separated by 11-coordinate barium cations.

In this paper, we report the synthesis, structure, and properties of $BaVO(PO_4)(H_2PO_4) \cdot H_2O$, a new layered barium vanadium(IV) phosphate hydrate. The V/P/O layer configuration in $BaVO(PO_4)(H_2PO_4) \cdot H_2O$ is related to that found in $VO(HPO_4) \cdot 4H_2O$ (8) and $VOPO_4 \cdot 2H_2O$ (9).

SYNTHESIS AND INITIAL CHARACTERIZATION

Numerous bluish-green, pseudo-hexagonal single crystals (to 0.5 mm) of $BaVO(PO_4)(H_2PO_4) \cdot H_2O$ were prepared from a reaction mixture comprising 2.0 ml (~20 mmol) 85% H_3PO_4, 1.09 g (5.52 mmol) $BaCO_3$, 0.50 g (2.75 mmol) V_2O_5, 0.045 g (0.88 mmol) V, and 6 ml H_2O (approximate Ba:V:P ratio = 1:1.2:3). The starting pH was adjusted to ~2.0 by the addition of 3 ml of 40% solution (in water) of tetraethylammonium hydroxide (TEAOH). The reactants were sealed in a 23-ml capacity Teflon-lined Parr hydrothermal bomb, which was approximately 45% full. The bomb was heated to 200°C for 4 days, and then slowly cooled to room temperature over a 2-day period. The bomb contents were recovered by vacuum filtration and drying in air. The yield of the title compound and other phases, including light blue rods of $Ba_8(VO)_6(HPO_4)_{11}(PO_4)_2 \cdot 3H_2O$ (6) and unidentified powder, was approximately 50%, of which an estimated 25% was $BaVO(PO_4)(H_2PO_4) \cdot H_2O$. Repeated attempts to hydrothermally prepare pure $BaVO(PO_4)(H_2PO_4) \cdot H_2O$ from a stoichiometric starting mixture of precursors (Ba:V:P ratio = 1:1:2) were unsuccessful and always resulted in a mixture of $BaVO(PO_4)(H_2PO_4) \cdot H_2O$, $Ba_8(VO)_6(HPO_4)_{11}(PO_4)_2 \cdot 3H_2O$, and other unknown phases. Reactions in which the initial pH adjustment was accomplished with NH_4OH rather than with TEAOH led to a complex, multiphase mixture of products, with no evidence for $BaVO(PO_4)(H_2PO_4) \cdot H_2O$ formation.

The distinct pseudo-hexagonal morphology of $BaVO(PO_4)(H_2PO_4) \cdot H_2O$ crystals allowed for hand sorting of enough pure crystalline material to carry out physical measurements, as follows.

Powder X-ray data for a thoroughly ground sample of $BaVO(PO_4)(H_2PO_4) \cdot H_2O$ (Scintag XDS2000 automated

0022-4596/95 $12.00

diffractometer, Cu$K\alpha$ radiation, λ = 1.5418 Å, flat-plate sample, θ-θ scan mode) could be indexed using the monoclinic cell parameters determined from the single-crystal experiment. A software "stripping" routine established peak positions relative to the Cu$K\alpha_1$ wavelength (λ = 1.5406 Å). Indices were assigned on the basis of a LAZY-PULVERIX (10) simulation of the $BaVO(PO_4)(H_2PO_4) \cdot H_2O$ structure, and after least-squares minimization, refined lattice parameters of a = 10.859 (7) Å, b = 6.404 (5) Å, c = 11.379 (7) Å, and β = 102.32(3)° (V = 773(5) Å^3) were obtained. The powder pattern of $BaVO(PO_4)(H_2PO_4) \cdot H_2O$ is listed in Table 1.

Thermogravimetric analysis (TGA) for $BaVO(PO_4)(H_2PO_4) \cdot H_2O$ was performed on a DuPont 2100 system: the sample was heated to 600°C at 3°C/min in a nitrogen atmosphere. X-ray powder diffraction on the greyish post-TGA residue indicated a complex pattern, different to that of $BaVO(PO_4)(H_2PO_4) \cdot H_2O$. Infrared data for $BaVO(PO_4)(H_2PO_4) \cdot H_2O$ were collected on a Galaxy FTIR 5000 Series spectrometer (KBr pellet method).

Magnetic susceptibility data for $BaVO(PO_4)(H_2PO_4) \cdot H_2O$, collected using ~23 mg single crystals, were obtained between 4.2 and 300 K (applied field 6 kG) using a Quantum Design model MPMS SQUID magnetometer. Ferromagnetic impurity contributions to the magnetic susceptibility were measured and corrected for by using magnetization isotherms obtained at 77 and 298 K.

TABLE 1
X-Ray Powder Data for $BaVO(PO_4)(H_2PO_4) \cdot H_2O$

h	k	l	d_{obs}(Å)	d_{calc}(Å)	Δd^a	I_{rel}^b
1	0	−1	8.642	8.652	−0.010	6
1	0	1	6.964	6.968	−0.005	5
1	1	0	5.478	5.482	−0.005	18
2	0	0	5.302	5.304	−0.002	14
1	1	−1	5.146	5.147	−0.001	22
2	0	−2	4.325	4.326	−0.001	18
2	1	0	4.083	4.085	−0.002	21
1	0	−3	3.756	3.757	−0.001	5
1	1	2	3.705	3.705	0.001	13
2	0	2	3.483	3.484	−0.002	8
1	0	3	3.286	3.287	−0.001	100
1	1	−3	3.243	3.240	0.003	11
3	0	1	3.192	3.180	0.013	30
3	1	−1	3.136	3.137	−0.001	6
3	1	0	3.095	3.096	−0.001	23
1	2	0	3.063	3.065	−0.002	15
2	1	−3	3.001	3.001	0.000	7
3	1	−2	2.948	2.949	−0.001	3
1	2	1	2.911	2.910	0.002	23
3	0	−3	2.886	2.884	0.002	19
0	2	2	2.778	2.775	0.003	8
1	2	−2	2.756	2.757	−0.001	11
2	2	−1	2.732	2.732	−0.001	6
4	0	0	2.652	2.652	−0.001	31
3	1	−3	2.631	2.630	0.001	9
2	2	1	2.597	2.596	0.001	26
0	1	4	2.551	2.550	0.001	11
3	1	2	2.511	2.512	−0.001	9
2	1	−4	2.495	2.497	−0.002	14
4	1	0	2.450	2.450	−0.001	5
4	1	−2	2.425	2.426	−0.001	11
4	1	1	2.299	2.300	−0.001	4
1	0	−5	2.276	2.276	0.000	6
3	1	3	2.183	2.184	−0.001	4
2	1	4	2.139	2.140	−0.001	5

[a] $d_{obs} - d_{calc}$.
[b] $100 \times I/I_{max}$.

STRUCTURE DETERMINATION

The crystal structure of $BaVO(PO_4)(H_2PO_4) \cdot H_2O$ was determined from single-crystal X-ray diffraction data: A blue-green hexagon (dimensions ~0.30 × 0.25 × 0.25 mm) was mounted on a thin glass fiber with cyanoacrylate adhesive, and room-temperature [25(2)°C] intensity data were collected on an Enraf–Nonius CAD4 automated 4-circle diffractometer (graphite-monochromated Mo$K\alpha$ radiation, λ = 0.71073 Å), as outlined in Table 2. 2301 intensity maxima were scanned ($2\theta < 60°$; $+h$, $+k$, $\pm l$), and the systematic absence conditions in the reduced data ($h0l$, $h + l \neq 2n$; $0k0$, $k \neq 2n$) uniquely indicated space group $P2_1/n$ (nonstandard setting of $P2_1/c$, No. 14). An absorption correction (min. = 2.33, max. = 2.98), based on ψ-scans of four reflections with $\chi \approx 90°$,

TABLE 2
Crystallographic Parameters for $BaVO(PO_4)(H_2PO_4) \cdot H_2O$

Empirical formula	$Ba_1V_1P_2O_{10}H_4$
Formula weight	414.24
Habit	Blue-green hexagon
Crystal system	Monoclinic
a (Å)	10.848(3)
b (Å)	6.408(3)
c (Å)	11.376(2)
β(°)	102.32(2)
V (Å^3)	773
Space group	$P2_1/n$ (No. 14)
Z	4
hkl limits	−15→14, 0→8, 0→15
T(°C)	25(1)
ρ_{calc} (g/cm^3)	3.56
μ(Mo$L\alpha$) (cm^{-1})	66.9
Min., max. $\Delta\rho$ (e/Å^3)	−1.4, 1.0
Total data	2301
Observed data[a]	1820
$R(F)$[b] (%)	2.24
$R_w(F)$[c] (%)	2.42

[a] $I > 3\sigma(I)$ after merging.
[b] $R = 100 \times \Sigma| |F_o| - |F_c| |/\Sigma|F_o|$.
[c] $R_w = 100 \times [\Sigma w(|F_o| - |F_c|)^2/\Sigma w|F_o|^2]^{1/2}$, with $w_i = 1/\sigma_i^2$.

was applied at the data reduction stage, along with the usual corrections for Lorentz and polarization effects. After merging to 2103 reflections (R_{Int} = 2.29%), 1820 of these were considered observable, based on the criterion $I > 3\sigma(I)$.

The crystal-structure model of $BaVO(PO_4)(H_2PO_4) \cdot H_2O$ was successfully developed in space group $P2_1/n$. Initial heavy-atom positions (Ba, V, P) were located using the direct-methods program SHELXS-86 (11), and oxygen-atom positions were located from Fourier difference maps during the refinement. A final difference synthesis clearly revealed four hydrogen-atom sites, and restraints [d(O–H) = 0.95(1) Å, θ(P–O–H) = 109(1)°] were used to stabilize the least-squares refinement of the H atom positions. The final cycles of full-matrix least-squares refinement were against F and included anisotropic temperature factors (atom type U_{iso} for H) and a Larson-type secondary extinction correction (12) [refined value: 2.8(4)]. Complex, neutral-atom scattering factors were obtained from the International Tables (13). At the end of the refinement, analysis of the various trends in F_o versus F_c revealed no unusual effects. The least-squares, Fourier, and subsidiary calculations were performed using the Oxford CRYSTALS system (14), running on a DEC MicroVAX 3100 computer. Final residuals of R = 2.24% and R_w = 2.42% ($w_i = 1/\sigma_i^2$) were obtained. Tables of anisotropic thermal parameters and observed and calculated structure factors are available from the authors.

RESULTS

Crystal structure. Final atomic positional and equivalent isotropic thermal parameters for $BaVO(PO_4)(H_2PO_4) \cdot H_2O$ are listed in Table 3, with selected bond distance/angle data given in Tables 4 and 5. The asymmetric unit and atom labeling scheme for $BaVO(PO_4)(H_2PO_4) \cdot H_2O$ are shown in Fig. 1, using ORTEP (15). $BaVO(PO_4)(H_2PO_4) \cdot H_2O$ is built up from barium cations, water molecules, and anionic sheets of vertex-sharing VO_6 and $(H_2)PO_4$ units. The complete crystal structure of $BaVO(PO_4)(H_2PO_4) \cdot H_2O$ is illustrated in Fig. 2.

The VO_6 group in $BaVO(PO_4)(H_2PO_4) \cdot H_2O$ is distorted and shows the short (d < 1.65 Å) terminal V(1)–O(1) "vanadyl" bond, characteristic of V^{IV}, as also observed in other BaVPO phases containing vanadium(IV) (6, 7). A longer V(1)–O(6) bond (d > 2.2 Å) is *trans* [θ[O(1)–V(1)–O(6)] = 176.2(1)°] to this short bond, and the other four V–O vertices are intermediate in length between these two extremes. V(1) makes five bonds to distinct, adjacent phosphorus atoms [2 × P(1) and 3 × P(2)], via V–O–P links (θ_{av} = 136.2°, standard deviation (SD) about mean = 11.3°). The average V–O bond length is 1.979(2) Å, and a Brese–O'Keeffe bond balance sum (BVS) calculation, based on the six individual V–O bond lengths (16), yields a value of 4.11, in good agreement with the value of 4.00 expected for a site with "pure" V^{IV} character.

The two distinct phosphorus atoms in $BaVO(PO_4)(H_2PO_4) \cdot H_2O$ are both tetrahedrally coordinated by oxygen atoms and show typical average geometrical parameters. For P(1), d_{av}(P–O) = 1.538(2) Å, BVS = 4.80, θ_{av}(O–P–O) = 109.4°, with SD of mean = 4.3°. For P(2),

TABLE 3
Atomic Positional Parameters for $BaVO(PO_4)(H_2PO_4) \cdot H_2O$

Atom	x	y	z	U_{eq}[a]
Ba(1)	0.65658(2)	0.14129(4)	−0.05498(2)	0.0107
V(1)	0.63251(6)	−0.0157(1)	0.31850(6)	0.0058
P(1)	0.34775(9)	−0.1194(2)	0.38455(9)	0.0077
P(2)	0.60393(9)	0.4978(2)	0.26340(9)	0.0058
O(1)	0.5992(3)	−0.0112(5)	0.1741(3)	0.0114
O(2)	0.6247(3)	0.2987(4)	0.3416(3)	0.0084
O(3)	0.4551(3)	−0.0327(5)	0.3360(3)	0.0145
O(4)	0.8199(3)	−0.0126(4)	0.3366(2)	0.0078
O(5)	0.6500(3)	−0.3220(4)	0.3505(2)	0.0068
O(6)	0.6921(3)	−0.0145(5)	0.5210(2)	0.0090
O(7)	0.2373(3)	−0.1520(5)	0.2716(3)	0.0124
O(8)	0.6240(3)	0.3462(5)	0.5638(3)	0.0133
O(9)	0.4656(3)	0.5256(5)	0.2010(2)	0.0088
O(10)	0.9314(3)	0.2486(5)	0.5181(3)	0.0121
H(7)	0.162(2)	−0.088(9)	0.283(3)	0.06(1)[b]
H(8)	0.616(6)	0.344(3)	0.479(1)	0.06(1)[b]
H(10)	0.956(6)	0.153(6)	0.582(3)	0.06(1)[b]
H(11)	0.892(5)	0.173(7)	0.449(3)	0.06(1)[b]

[a] U_{eq}(Å²) = $(U_1\ U_2\ U_3)^{1/3}$
[b] Atom type U_{iso} (Å²).

TABLE 4
Bond Distances (Å) for $BaVO(PO_4)(H_2PO_4) \cdot H_2O$

Ba(1)–O(1)	2.971(3)	Ba(1)–O(1)	2.937(3)
Ba(1)–O(5)	2.790(3)	Ba(1)–O(6)	2.728(3)
Ba(1)–O(7)	2.935(3)	Ba(1)–O(8)	3.058(3)
Ba(1)–O(9)	2.852(3)	Ba(1)–O(10)	2.755(3)
Ba(1)–O(10)	2.833(3)		
V(1)–O(1)	1.605(3)	V(1)–O(2)	2.036(3)
V(1)–O(3)	1.980(3)	V(1)–O(4)	1.999(3)
V(1)–O(5)	1.998(3)	V(1)–O(6)	2.256(3)
P(1)–O(3)	1.498(3)	P(1)–O(6)	1.508(3)
P(1)–O(7)	1.572(3)	P(1)–O(8)	1.574(3)
P(2)–O(2)	1.544(3)	P(2)–O(4)	1.544(3)
P(2)–O(5)	1.534(3)	P(2)–O(9)	1.527(3)
O(2)–H(8)[a]	1.62(1)	O(4)–H(11)[a]	1.80(1)
O(7)–H(7)	0.95(1)	O(8)–H(8)	0.95(1)
O(9)–H(7)[a]	1.61(1)	O(9)–H(10)[a]	1.76(2)
O(10)–H(10)	0.95(1)	O(10)–H(11)	0.94(1)

[a] H-bond contact.

TABLE 5
Selected Bond Angles(°) for $BaVO(PO_4)(H_2PO_4) \cdot H_2O$

O(1)–V(1)–O(2)	96.2(1)	O(1)–V(1)–O(3)	95.3(1)
O(2)–V(1)–O(3)	88.5(1)	O(1)–V(1)–O(4)	96.1(1)
O(2)–V(1)–O(4)	92.6(1)	O(3)–V(1)–O(4)	168.3(1)
O(1)–V(1)–O(5)	101.3(1)	O(2)–V(1)–O(5)	162.5(1)
O(3)–V(1)–O(5)	89.1(1)	O(4)–V(1)–O(5)	86.3(1)
O(1)–V(1)–O(6)	176.2(1)	O(2)–V(1)–O(6)	82.8(1)
O(3)–V(1)–O(6)	88.3(1)	O(4)–V(1)–O(6)	80.3(1)
O(5)–V(1)–O(6)	79.8(1)		
O(3)–P(1)–O(6)	114.5(2)	O(3)–P(1)–O(7)	105.3(2)
O(6)–P(1)–O(7)	111.9(2)	O(3)–P(1)–O(8)	112.1(2)
O(6)–P(1)–O(8)	108.8(2)	O(7)–P(1)–O(8)	103.6(2)
O(2)–P(2)–O(4)	110.7(2)	O(2)–P(2)–O(5)	105.2(2)
O(4)–P(2)–O(5)	110.9(2)	O(2)–P(2)–O(9)	111.9(2)
O(4)–P(2)–O(9)	106.8(2)	O(5)–P(2)–O(9)	111.4(2)
V(1)–O(2)–P(2)	138.4(2)	V(1)–O(3)–P(1)	155.0(2)
V(1)–O(4)–P(2)	128.1(2)	V(1)–O(5)–P(2)	128.1(2)
V(1)–O(6)–P(1)	131.8(2)	P(1)–O(7)–H(7)	111.2(10)
P(1)–O(8)–H(8)	109.6(10)		
O(7)–H(7)–O(9)[a]	178.0(61)	O(2)[a]–H(8)–O(8)	167.1(33)
O(9)–H(10)–O(10)[a]	166.8(58)	O(4)[a]–H(11)–O(10)	169.4(47)

[a] H-bond contact.

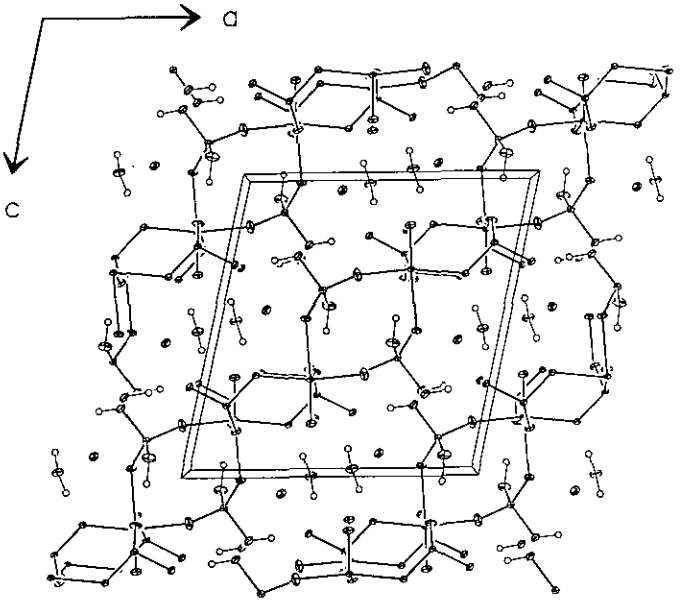

FIG. 2. Unit-cell packing of $BaVO(PO_4)(H_2PO_4) \cdot H_2O$, viewed down [010], showing the infinite $VO(PO_4)(H_2PO_4)$ sheets, separated by Ba^{2+} cations and O(10)/H(10)/H(11) water molecules (50% thermal ellipses).

d_{av}(P–O) = 1.537(2) Å, BVS = 4.79, θ_{av}(O–P–O) = 109.4°, with SD of mean = 2.8°. P(1) makes two P(1)–O–V bonds [via O(3) and O(6)] and two P–OH links [O(7) and O(8)], with the latter P–OH bond type showing its typical lengthening relative to P–O bonds (17) (Table 4). These protons are both involved in H-bonds (*vide infra*). P(2) makes three P–O–V links [O(2), O(4), O(5)], and one terminal P–O(9) link, which partakes in two P–O(9) · · · H H-bond links, as described below.

The barium cation in $BaVO(PO_4)(H_2PO_4) \cdot H_2O$ is 9-coordinate to oxygen atoms within 3.2 Å, two of which are vanadyl V(1)=O(1) atoms and two of which are water-molecule O(10) atoms. An irregular geometry (Fig. 3) results, with a d_{av}(Ba–O) of 2.873(2) Å and a BVS[Ba(1)] of 1.93 (expected = 2.00). Barium appears to have no special coordination requirements in vanadium(IV)-containing BaVPOs, and its coordination number ranges from 9 in $BaVO(PO_4)(H_2PO_4) \cdot H_2O$ to 13 for one of the Ba sites in $Ba_8(VO)_6(HPO_4)_{11}(PO_4)_2 \cdot 3H_2O$ (6).

All four protons in $BaVO(PO_4)(H_2PO_4) \cdot H_2O$ are involved in H bonds (Tables 4 and 5). O(7)–H(7) · · · O(9) forms an interlayer connection, while the O(8)–H(8) · · · O(2) bond is an in-layer link. The water molecule [oxygen

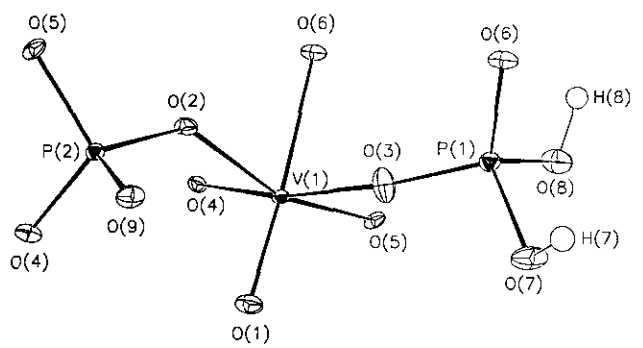

FIG. 1. Detail of the asymmetric unit of $BaVO(PO_4)(H_2PO_4) \cdot H_2O$, showing atom labeling scheme (50% thermal ellipsoids).

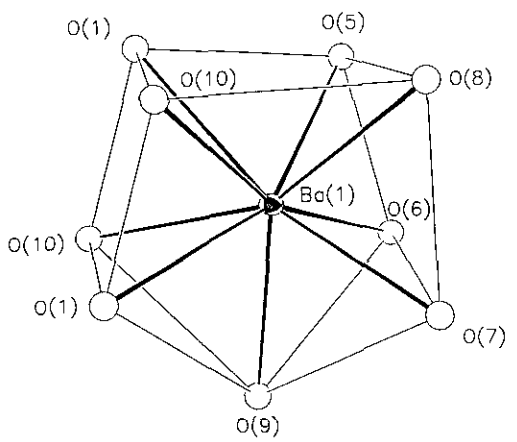

FIG. 3. 9-coordinate Ba(1) coordination polyhedron in $BaVO(PO_4)(H_2PO_4) \cdot H_2O$, with nonbonding O · · · O contacts < 3.8 Å indicated by thin lines. O-atoms are represented by spheres of arbitrary radius.

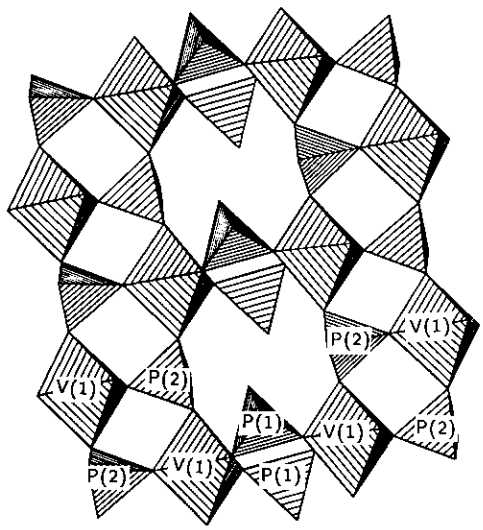

FIG. 4. STRUPLO polyhedral plot of a section of the infinite VO $(PO_4)(H_2PO_4)$ sheet structure in $BaVO(PO_4)(H_2PO_4) \cdot H_2O$, showing "8-rings" of VO_6 and PO_4 polyhedra (see text). View is approximately down [101].

atom O(10)] plays an important role in separating the $VO(PO_4)(H_2PO_4)$ sheets, as an O(4) $\cdots$ H(11)–O(10)–H(10) $\cdots$ O(9) bridge.

The structural motif in $BaVO(PO_4)(H_2PO_4) \cdot H_2O$ is dominated by anionic sheets [stoichiometry $VO(PO_4)(H_2PO_4)$], which are aligned roughly in the [101] crystallographic plane. These sheets are built up from double chains of V(1)/P(2)-centered groups, which propagate in the **b**-direction. $H_2P(1)O_4$ groups crosslink the double chains into a two-dimensional structure, resulting in infinite sheets containing "8-ring" (4 V + 4 P nodes) holes (Fig. 4). Comparable V/P/O sheet structures are briefly described below.

TGA measurements. A complex, multistage weight-loss scheme was observed for $BaVO(PO_4)(H_2PO_4) \cdot H_2O$, with a definite plateau at ~300°C (1.44% observed weight loss) and an overall weight loss of 8.90%, complete by 600°C. The first plateau may correspond to partial water loss from $BaVO(PO_4)(H_2PO_4) \cdot H_2O$, while the overall observed weight loss (calc. = 8.70%) is in good agreement with loss of all the hydrogen (as water) from $BaVO(PO_4)(H_2PO_4) \cdot H_2O$, as

$$BaVO(PO_4)(H_2PO_4) \cdot H_2O \xrightarrow{\Delta} \text{"}BaVP_2O_8\text{"} + 2H_2O.$$

Infrared measurements. The IR data for $BaVO(PO_4)(H_2PO_4) \cdot H_2O$ (Fig. 5) show typical bands associated with V–O and P–O resonances, as well as characteristic signals due to water molecule vibrations. PO_4 and V=O resonances both occur in the 800–1000 cm^{-1} region, and without further measurements, definitive assignments cannot be made (18). A typical broad band due to O–H stretches in a coordinated water molecule occurs at ~3223 cm^{-1}. The sharp bands at 1199 and 1309 cm^{-1} are probably dihydrogen phosphate P–OH modes and occur at slightly higher frequencies than similar bands observed in the normal salt NaH_2PO_4 (19).

Magnetic measurements. Inverse susceptibility data for $BaVO(PO_4)(H_2PO_4) \cdot H_2O$ (Fig. 6) show perfect Curie–Weiss-type paramagnetic behavior over the entire ~4–300 K range. The data were modeled by the function $\chi = \chi_0 + C/(T - \theta)$, where χ is the measured magnetic susceptibility, C the Curie constant, T the temperature (K), and θ the Weiss constant. The model yielded best-fit values of $\chi_0 = -4.22 \times 10^{-7}$ emu/g, $C = 9.308 \times 10^{-4}$ emu-K/g, and $\theta = 0.9$ K, corresponding to a μ_{eff} of 1.69 μ_B in good agreement with the ideal spin-only value of 1.73 μ_B for d^1-vanadium(IV).

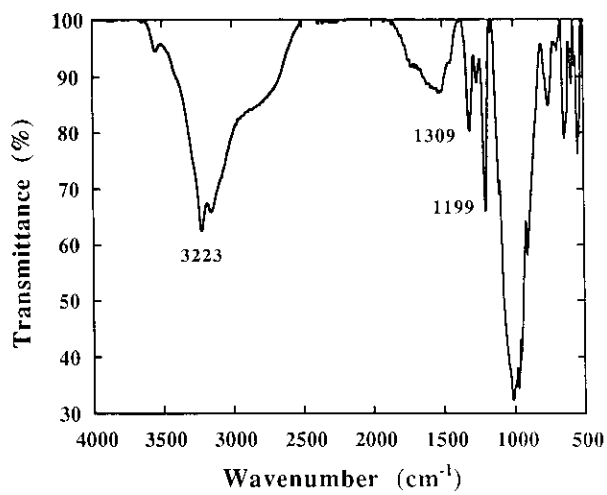

FIG. 5. Infrared spectrum of $BaVO(PO_4)(H_2PO_4) \cdot H_2O$.

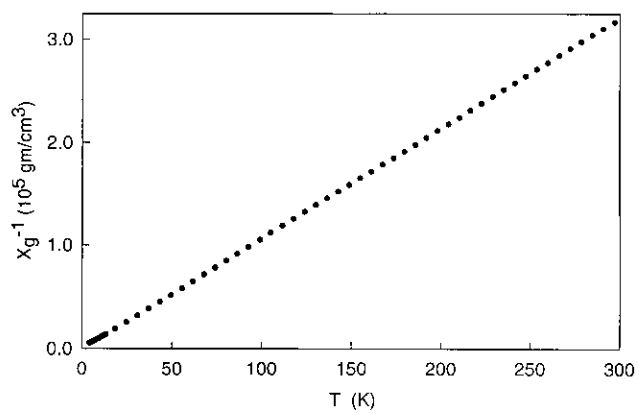

FIG. 6. Magnetic susceptibility data for $BaVO(PO_4)(H_2PO_4) \cdot H_2O$, plotted as $1/\chi$ versus temperature.

CONCLUSION

The new barium vanadium(IV) phosphate, $BaVO(PO_4)(H_2PO_4) \cdot H_2O$, shows a distorted VO_6 geometry similar to that seen in other BaVPO phases containing V^{IV}, but the polyhedral connectivity of VO_6 and $(H_2)PO_4$ units leads to a anionic V/P/O layer structure in this material, unlike the one-dimensional motifs observed in $Ba_8(VO)_6(HPO_4)_{11}(PO_4)_2 \cdot 3H_2O$ (6) and $BaVO(PO_4)(H_2PO_4) \cdot H_2O$ (7). Pure V^{IV} character is well defined for the vanadium center in $Ba_2VO(PO_4)_2 \cdot H_2O$ (crystal color, bond–valence–sum calculations, magnetic susceptibility data).

Tetraethylammonium hydroxide is required in the reaction mixture, but is not incorporated into the $BaVO(PO_4)(H_2PO_4) \cdot H_2O$ product. Conversely, the use of ammonium hydroxide to adjust pH leads to other, unknown phases. The two new adamite-type phases, $Co_2(OH)PO_4$ and $Zn_2(OH)PO_4$, recently reported (20) were also prepared hydrothermally (as single crystals) in the presence of bulky organic bases, and the use of ammonium hydroxide led to other phases.

The "checkerboard" V/P/O layer motif in $BaVO(PO_4)(H_2PO_4) \cdot H_2O$ is related to V/P/O arrangements in other vanadium/phosphate phases. The V^{IV}-containing $VO(HPO_4) \cdot 4H_2O$ (8) contains one-dimensional double VO_6/PO_4 chains, very similar to the V(1)/P(2) chains in $BaVO(PO_4)(H_2PO_4) \cdot H_2O$. In $VO(HPO_4) \cdot 4H_2O$, the chains are not linked together by bridging dihydrogen phosphate groups, but are separated by water molecules and only connected via H bonds. $(VO)_3(PO_4)_2 \cdot 9H_2O$ (21) [vanadium(IV)], which was characterized by *ab initio* structure solution from X-ray powder data, also contains V/P/O layers incorporating 8-ring holes, occupied by water molecules, akin to those found in $BaVO(PO_4)(H_2PO_4) \cdot H_2O$. However, the $(VO)_3(PO_4)_2 \cdot 9H_2O$ layers are condensed into a three-dimensional vanadophosphate framework.

Related layered V/P/O phases include α-$VO(HPO_4) \cdot 2H_2O$ (22), which contains V–O–V links, and β-$VO(HPO_4) \cdot 2H_2O$ (23), which contains squashed 8-rings and zigzag double VO_6/PO_4 chains. $VOPO_4 \cdot 2H_2O$ [vanadium(V)] (9) contains a regular $VO_6/PO4$ array, linked by V–O–P bonds, without vacancies, while $VO(H_2PO_4)_2$ (24, 25) contains V atom "vacancies" in its V–O–P connected sheet structure, somewhat like those in the presently studied phase. However, in $VO(H_2PO_4)_2$, the sheets are linked into a three-dimensional structure by V–O=V links.

ACKNOWLEDGMENTS

We thank Ivan Bernal (University of Houston) for access to X-ray data collection facilities. This work is partially funded by the National Science Foundation (DMR-9214804) and the Welch Foundation.

REFERENCES

1. H. Y. Yang, S. L. Wang, and K. H. Lii, *Acta Crystallogr. Sect. C* **48,** 975 (1992).
2. A. Grandin, J. Chardon, M. M. Borel, A. LeClair, and B. Raveau, *J. Solid State Chem.* **99,** 297 (1992).
3. L. Benhamada, A. Grandin, M. M. Borel, A. LeClair, and B. Raveau, *Acta Crystallogr. Sect. C* **47,** 2438 (1991).
4. E. Dvoncova, K.-H. Lii, C.-H. Li, and T.-M. Chen. *J. Solid State Chem.* **106,** 485 (1993).
5. Z. Wang, R. C. Haushalter, M. E. Thompson, and J. Zubieta, *Mater. Chem. Phys.* **35,** 205 (1993).
6. W. T. A. Harrison, J. T. Vaughey, A. J. Jacobson, D. P. Goshorn, and J. W. Johnson, *J. Solid State Chem.* **116,** 77 (1995).
7. W. T. A. Harrison, S. C. Lim, J. T. Vaughey, A. J. Jacobson, D. P. Goshorn, and J. W. Johnson, *J. Solid State Chem.* **113,** 444 (1994).
8. M. E. Leonowicz, J. W. Johnson, J. F. Brody, H. F. Shannon H F, and J. M. Newsam, *J. Solid State Chem.* **56,** 370 (1985).
9. H. R. Tietze, *Aust. J. Chem.* **34,** 2035 (1981).
10. K. Yvon, W. Jeitscho, and E. Parthe, *J. Appl. Crystallogr.* **10,** 73 (1977).
11. G. M. Sheldrick, "SHELXS-86 User Guide." Crystallography Department, University of Göttingen, Germany, 1986.
12. A. C. Larson, *Acta Crystallogr.* **23,** 664 (1967).
13. "International Tables for X-Ray Crystallography," Vol. IV. Kynoch Press, Birmingham, UK, 1974.
14. D. J. Watkin, J. R. Carruthers, and P. W. Betteridge, "CRYSTALS User Guide, Version 9.0," Chemical Crystallography Laboratory, Oxford University, UK (1993).
15. C. K. Johnson, Report ORNL-5138, Oak Ridge National Laboratory, Oak Ridge, Tennessee, 1976, with local modifications.
16. N. E. Brese and M. O'Keeffe, *Acta Crystallogr. Sect. B* **47,** 192 (1991).
17. W. T. A. Harrison, T. M. Nenoff, M. M. Eddy, T. E. Martin, and G. D. Stucky, *J. Mater. Chem.* **2,** 1127 (1992).
18. J. W. Johnson, A. J. Jacobson, J. F. Brody, and S. M. Rich, *Inorg. Chem.* **21,** 3820 (1982).
19. A. C. Chapman and L. E. Thirwell, *Spectrochim. Acta* **20,** 937 (1964).
20. W. T. A. Harrison, J. T. Vaughey, L. L. Dussack, A. J. Jacobson, T. E. Martin, and G. D. Stucky, *J. Solid State Chem.* **114,** 151 (1995).
21. R. G. Teller, P. Blum, E. Kostiner, and J. A. Hriljac, *J. Solid State Chem.* **97,** 10 (1992).
22. A. Le Bail, G. Ferey, P. Aramos, and D. Beltran-Porter, *Eur. J. Solid State Inorg. Chem.* **26,** 419 (1989).
23. A. Le Bail, G. Ferey, P. Aramos, D. Beltran-Porter, and G. Villeneuve, *J. Solid State Chem.* **79,** 169 (1989).
24. S. A. Linde, Y. E. Gorbunova, A. V. Lavrov, and V. G. Kusnetzov, *Dokl. Akad. Nauk SSSR* **224,** 1711 (1979).
25. G. Villeneuve, A. Erragh, D. Beltran, M. Drillon, and P. Hagenmuller, *Mater. Res. Bull.* **21,** 621 (1986).